Journal of Solid State Chemistry **163,** 239–247 (2002)
doi:10.1006/jssc.2001.9398, available online at http://www.idealibrary.com on IDEAL®

Preparation of (111)-Oriented Epitaxial $Fe_{3-x}O_4$ Films on α-Al_2O_3 (0001) Substrates by Coating-Pyrolysis Process Using Postepitaxial Topotaxy via (0001)-Oriented α-Fe_2O_3

Iwao Yamaguchi, Tsuyoshi Terayama,* Takaaki Manabe, Tetsuo Tsuchiya, Mitsugu Sohma, Toshiya Kumagai, and Susumu Mizuta

*National Institute of Advanced Industrial Science and Technology (AIST), Higashi 1-1, Tsukuba, Ibaraki 305-8565, Japan; and *Chiba Institute of Technology, Narashino 2-17-1, Chiba 275-0016, Japan*

Received June 15, 2001; in revised form September 5, 2001; accepted September 14, 2001; published online November 27, 2001

We have succeeded in preparing the (111)-oriented epitaxial films of magnetite (Fe_3O_4) and maghemite (γ-Fe_2O_3), or $Fe_{3-x}O_4$, on the C-planes of sapphire [α-Al_2O_3(0001)] by a coating-pyrolysis (CP) process using postepitaxial topotaxy (PET). In this set of film and substrate, not only the structure type is different, i.e., the cubic spinel type versus hexagonal corundum type, but the lattice mismatch is large, i.e., 8.0%. The PET process consists of one epitaxial growth and one or more topotactic reaction steps. In the present work, a (0001)-oriented epitaxial film of hematite (α-Fe_2O_3) [corundum-type iron (III) oxide] was first formed on an α-Al_2O_3(0001) substrate by CP process. Second, α-Fe_2O_3 was reduced to Fe_3O_4 in a gas flow of an argon–hydrogen gas mixture with a hydrogen partial pressure of 0.023 atm. Finally, the Fe_3O_4 was oxidized in air to γ-Fe_2O_3, or $Fe_{3-x}O_4$. Pole-figure analysis exhibited that both the products, Fe_3O_4 and γ-Fe_2O_3, were (111)-oriented and epitaxially grown on the substrate surface. The crystallographic relationship is Fe_3O_4, γ-Fe_2O_3 (111) $\|\alpha$-Al_2O_3 (0001) and Fe_3O_4, γ-Fe_2O_3 [$1\bar{1}0$]$\|\alpha$-Al_2O_3 $\langle 1\bar{1}00\rangle$, $\langle\bar{1}100\rangle$. This implies that α-Fe_2O_3(0001) has been topotactically converted to Fe_3O_4(111) and γ-Fe_2O_3(111). Magnetic properties and surface morphology of the films were also investigated using SQUID and atomic force microscopy, respectively.

Key Words: **topotaxy; epitaxial film; coating pyrolysis; redox reaction; hematite; magnetite; maghemite; pole figure.**

INTRODUCTION

Epitaxial metal oxide films are being expected for use in a variety of electronic and magnetic applications (1). Among various techniques for fabrication of epitaxial oxide films, chemical solution-based processes like the sol-gel method and a coating-pyrolysis (CP) process, or metal organic deposition (MOD), are noted as being less expensive and suitable for large-scale production. We have been preparing epitaxial films of various functional oxide, such as superconductor (2), ferroelectric (3), and magnetic (4) materials by this process. However, when crystal structures are different or the lattice misfit is large between the film and the substrate materials, growth of epitaxial films is considerably difficult by these chemical solution-based processes. This arises from the fact that the microstructure of the product layer is chiefly governed by thermodynamic factors rather than by kinetic factors; that is, the CP is essentially an *ex situ* process, in which a precursor layer is transformed into a product film through high-temperature annealing.

In this article, we will introduce a new idea of preparing an epitaxial (111)-oriented magnetite (Fe_3O_4) films on sapphire (α-Al_2O_3), which has been difficult to fabricate especially by the solution-related processes. Before doing so, we summarize the structures and lattice constants of relevant iron oxides and substrate materials in Table 1 and the previous work on epitaxial growth of Fe_3O_4 and hematite (α-Fe_2O_3) films. Table 1 shows that Fe_3O_4 has a spinel-type structure, $Fd3m$, with a face-centered cubic (fcc) oxide anion sublattice. Therefore, epitaxial Fe_3O_4 films have chiefly been grown on MgO (5–7), in which oxide anion sublattice is the same as the spinel structure, i.e., fcc, and the lattice mismatch between them is so small, -0.3%. Similarly, the crystal structure of α-Fe_2O_3; i.e., rhombohedral corundum structure, $R\bar{3}c$, is the same as α-Al_2O_3, in which oxide anion sublattice is hexagonal close packing (hcp). It is easy to obtain epitaxial α-Fe_2O_3 films on α-Al_2O_3 because these structures are the same, although the lattice mismatch is comparatively large, 5.8%. Thus, epitaxial α-Fe_2O_3 films on α-Al_2O_3 substrates were prepared by not only gas-phase methods (5) but solution-related methods (8, 9). In contrast, when the crystal structures of the film and the substrate materials are different, epitaxial (111)-oriented Fe_3O_4 films on α-Al_2O_3(0001) (5, 6, 10–12) or Pt(111) (13–15), for example, were fabricated only by gas-phase deposition methods. There have been no reports on the preparation of epitaxial (111)-oriented Fe_3O_4 films on these substrates by

0022-4596/02 $35.00

TABLE 1
The Structures and Lattice Constants of Magnetite (Fe_3O_4), Hematite (α-Fe_2O_3), MgO, and Sapphire (α-Al_2O_3)

	Structure (space group)	Lattice constants[a] (nm)	Oxide anion sublattice	Oxide anion layer order	Oxide anion distance[b] (nm)	Mismatch with α-Al_2O_3[c]	Mismatch with MgO[d]
Fe_3O_4	Spinel ($Fd3m$)	$a = 0.8396$	fcc	ABCABC	0.2968	8.0%	− 0.3%
α-Fe_2O_3	Corundum ($R\bar{3}c$)	$a = 0.5036$, $c = 1.3749$	hcp	ABABAB	0.2908	5.8%	
MgO	Rock salt ($Fm3m$)	$a = 0.4211$	fcc	ABCABC	0.2978		
α-Al_2O_3	Corundum ($R\bar{3}c$)	$a = 0.4759$, $c = 1.2993$	hcp	ABABAB	0.2748		

[a]Hexagonal indice for corundum structure.
[b]Average values in oxide anion layers estimated from lattice constants.
[c]Fe_3O_4(111) and α-Fe_2O_3(0001) films relative to α-Al_2O_3(0001) substrate.
[d]Fe_3O_4(100) and (111) films relative to MgO(100) and (111) substrates, respectively.

chemical solution methods to the best of our knowledge. This may be attributed to the structural difference and large lattice mismatch between Fe_3O_4(111) and α-Al_2O_3(0001), i.e., 8.0%, estimated from the average distance between the nearest neighboring oxide anions.

Recently, we investigated the growth behavior of epitaxial films in the CP process using one-component metal oxide systems, Fe–O (8.16) and V–O (17), in which the atmosphere of pyrolysis of metal organic compounds as well as that of the subsequent high-temperature heat treatment influences the extent of epitaxy. For example, in the growth of α-Fe_2O_3 films on α-Al_2O_3 substrates (16), highly epitaxial films were obtained when prefiring was carried out at a temperature corresponding to the removal of most of the organic component from the precursor prior to the formation of metal oxide crystallites. Also, the extent of in-plane alignment of α-Fe_2O_3 films was degraded when they were prepared via the Fe_3O_4 phase, which occurred in a reductive atmosphere due to the decomposition of organic component. Moreover, in the V–O system (17), we noticed the occurrence of twins in epitaxial V_2O_3 films on α-Al_2O_3 and attributed it to the topotactic reduction of VO_2 that formed during pyrolysis or heat treatment. Therefore, in general, the formation of an intermediate phase has been thought disadvantageous for producing an epitaxial film of the expected phase. From the latter negative results, however, we found a new idea of preparing an epitaxial (111)-oriented Fe_3O_4 film on α-Al_2O_3(0001), which has been difficult to fabricate by solution-related processes as mentioned earlier. The point is that the transformation of an intermediate phase is effectively used to obtain the expected product phase, i.e., topotactic reduction of an epitaxial α-Fe_2O_3(0001) film. We call such a route a postepitaxial topotactic (PET) process, which consists of a set of epitaxial growth of one phase and its subsequent conversion to another phase by one or more topotactic reactions.

Meanwhile, epitaxial Fe_3O_4 films with varied orientations are expected for use in elucidating the catalyst mechanism (13) and in high-density recording media with perpendicular magnetization (18). Thus, it is quite interesting to grow an epitaxial film of Fe_3O_4 on various substrates, especially, on lattice-misfit substrate surfaces. Since solution-related routes have the possibility of providing particles with varying shapes and sizes, like acicular β-FeOOH particles precipitated from an aqueous solution (19), and the CP process sometimes produces porous films due to rapid elimination of organic component, it is expected that perpendicularly magnetized films with columnar grains or catalyst films with higher specific surface areas be obtained. Therefore, we tried to prepare an epitaxial Fe_3O_4(111) film on α-Al_2O_3(0001) by the CP process. Furthermore, it is well known that acicular α-Fe_2O_3 particles are firstly reduced to acicular Fe_3O_4 and then reoxidized for manufacturing the acicular maghemite (γ-Fe_2O_3) particles for use in magnetic recording media (20, 21). Thus, we also report that epitaxial γ-Fe_2O_3 films can be obtained by topotactic reoxidation of epitaxial Fe_3O_4 films produced by PET process. We discuss as well some results of magnetization measurement using SQUID and of surface morphology using atomic force microscopy (AFM) of the films.

EXPERIMENTAL

An iron 2-ethylhexanoate solution diluted with mineral spirit (Nihon Kagaku Sangyo Co., Ltd.) was spin-coated (2000 rpm, 5 s) onto C-plane of sapphire substrates, α-Al_2O_3(0001). The coated films were prefired in air at 300°C for 1 h. First, the prefired film was heat-treated in a CO–CO_2 gas mixture ($pCO/pCO_2 = 10^{-1}$) at 600°C for 2 h to find out if an epitaxial Fe_3O_4 film directly forms from the amorphous precursor film.

Next, we tried to prepare epitaxial Fe_3O_4 films via epitaxial α-Fe_2O_3 films that can be obtained by heat treatment of the prefired films at 800°C for 2 h in a stream of air. The epitaxial α-Fe_2O_3 films were reduced in a flow of a CO–CO_2 gas mixture ($pCO/pCO_2 = 10^{-1}$, 400–600°C) for 4 h or in a gas flow of a hydrogen–argon mixture ($pH_2 = 0.023$ atm, 200–600°C) for 4 h. The latter condition

is strongly reductive, whereas the former condition is in the Fe_3O_4 stable region. Then, the Fe_3O_4 films were oxidized at 250–400°C for 2 h in a stream of air to γ-Fe_2O_3 and α-Fe_2O_3. Film thickness was evaluated from the weight change to be 300–500 nm.

The phases and orientations of the product films were confirmed by the conventional XRD θ–2θ scanning and pole-figure analysis by the Schulz reflection method, using the Cu$K\alpha_1$ line (MAC Science Co., Ltd. X-ray diffractometer MXP^{3A} with a pole-figure attachment). The pole-figure measurement was carried out on the $10\bar{1}4$ reflection of α-Fe_2O_3 and on the 400 reflection of spinel oxides (Fe_3O_4, γ-Fe_2O_3). Magnetic properties were measured by SQUID magnetometer (Quantum Design, MPMS-7). In this measurement, magnetization per gram of an α-Al_2O_3 substrate without film was first measured as standard. The magnetization per gram of film was evaluated by subtracting the magnetization due to the substrate estimated with the weight of the substrate. Surface morphology of the films was observed by atomic force microscopy (AFM, Digital Instruments, Nanoscope IIIa).

RESULTS AND DISCUSSION

A. Heat Treatment of Prefired Films

Figure 1 shows XRD θ–2θ scan profiles for the films obtained after the as-prefired amorphous precursor films were heat-treated under various conditions (atmosphere and temperature) for 2 h; (a) α-Fe_2O_3 film (air, 800°C), (b) Fe_3O_4 film (pCO/pCO$_2$ = 10^{-1}, 600°C), and (c) Fe film (pH$_2$ = 0.023 atm, 600°C). These conditions correspond to the stable regions of the respective product phases (22). It is clearly seen in Fig. 1a that a (0001)-oriented α-Fe_2O_3 film was obtained since the 0006 peak of α-Fe_2O_3 appeared at the low-angle side of that of α-Al_2O_3 substrate. On the other hand, the XRD pattern for the Fe_3O_4 film resembles the powder pattern except for the substrate's peaks (Fig. 1b). The formation of nonoriented Fe_3O_4 is ascribed to a very large mismatch (8.0%) between Fe_3O_4(111) and α-Al_2O_3(0001). Figure 1c shows that metal iron will precipitate at this temperature in the atmosphere that we use in the reduction treatment as referred to below.

B. Reduction of Epitaxial α-Fe_2O_3 Films to Fe_3O_4 Films

These results show that direct production of an epitaxial film of Fe_3O_4 from an as-prefired amorphous precursor is very difficult. Therefore, we tried to prepare an epitaxial Fe_3O_4 film via an epitaxial α-Fe_2O_3 film by reductive conversion. First, the epitaxial α-Fe_2O_3 film was reduced in a CO–CO_2 gas mixture (pCO/pCO$_2$ = 10^{-1}) that corresponds to an atmosphere in which the Fe_3O_4 phase is stable. However, epitaxial Fe_3O_4 films were not obtained under these conditions. According to XRD measurement (not shown), neither α-Fe_2O_3 000l nor Fe_3O_4 *hhh* peaks were observed in the films reduced at 400–600°C, except for the Fe_3O_4 311 peak, which is the most intense peak in the powder pattern, for the film reduced at 600°C. Thus, we tried to reduce the α-Fe_2O_3 films using a more reducing atmosphere (pH$_2$ = 0.023 atm) that corresponds to the region in which Fe_3O_4 is unstable. Figure 2 shows XRD θ–2θ scan profiles for the films reduced in the Ar–H_2 mixed gas

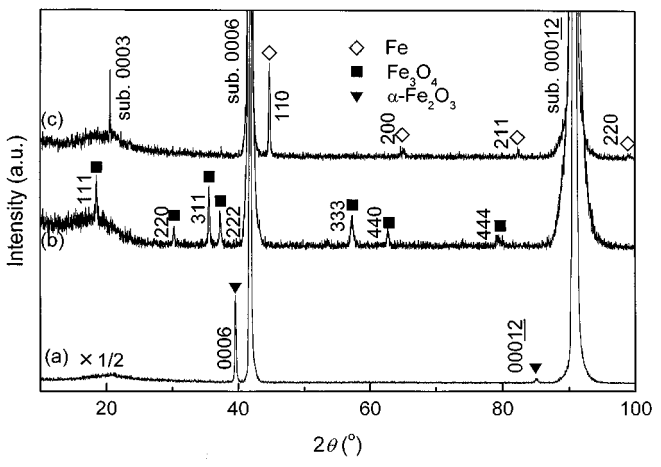

FIG. 1. XRD patterns of films after heat treatments of amorphous precursors at (a) 800°C in air, (b) 600°C in CO–CO_2 gas mixture (pCO/pCO$_2$ = 10^{-1}), and (c) 600°C in H_2–Ar gas mixture (pH$_2$ = 0.023 atm).

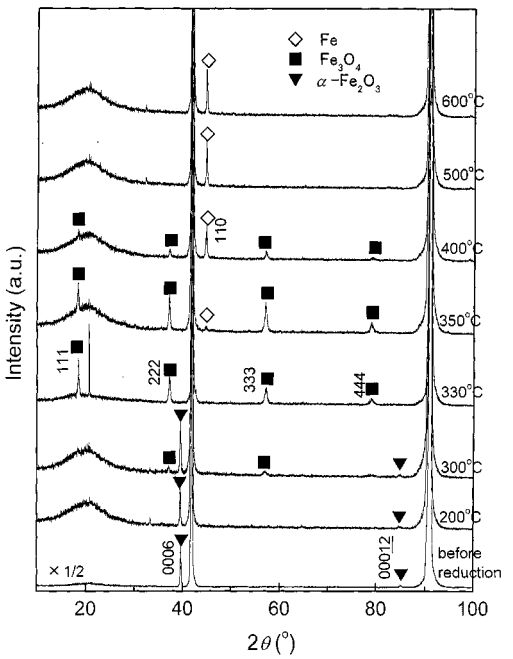

FIG. 2. XRD patterns of films before and after reduction of the epitaxial α-Fe_2O_3(0001) film at 200–600°C in H_2–Ar gas flow (pH$_2$ = 0.023 atm).

($pH_2 = 0.023$ atm) flow at 200–600°C as well as that of the film before reduction. It is clearly shown that the (111)-oriented Fe_3O_4 grains have grown after reduction in the temperature range 300–400°C, whereas metal iron is formed after reduction at 350°C and higher. The film that contains Fe_3O_4 alone was obtained by heat treatment only at 330°C. The color of the specimen, black, suggests the formation of Fe_3O_4 rather than that of γ-Fe_2O_3, of which the color is dark brown. The reducing atmosphere in this case is so strong that the optimum temperature region for occurrence of Fe_3O_4 becomes very narrow. One might think that it would be easier to control the temperature if we use a flow of a less reductive gas. However, a milder reducing atmosphere using a CO–CO_2 mixture ($pCO/pCO_2 = 10^{-1}$, 400°C), which corresponds to the Fe_3O_4 stable region, was found to be insufficient for reduction of α-Fe_2O_3 to Fe_3O_4.

C. *Oxidation of Epitaxial Fe_3O_4 Films to Epitaxial γ-Fe_2O_3 Films*

Subsequently, the epitaxial Fe_3O_4 films were oxidized in a stream of air at 250–400°C for 2 h. Figure 3 shows XRD θ–2θ scan profiles for the product films together with the Fe_3O_4 film before oxidation. It is found that the (111)-oriented spinel structure can be preserved after oxidation below 300°C and that the α-Fe_2O_3 grains reappeared by oxidation at 350°C and higher. Peaks at $2\theta = 23.8°$, 26.7° corresponding to the compound for attaching the the sample to the holder and peaks at $2\theta = 20.5°$ and 64.5° corresponding to the α-Al_2O_3 003 and 009 reflections, respectively, were observed in scan profiles of some specimens. The lattice parameters of Fe_3O_4 and γ-Fe_2O_3 evaluated from the d values of the 222 peaks by assuming the strain-free cubic structure decreased from 0.8385 to 0.8329 nm after oxidation at 300°C. The lattice parameter of γ-Fe_2O_3 was slightly smaller than that according to the ICDD data (39–1346), i.e., 0.8352 nm. However, this value is reasonable because one third of the parameter of superlattices according to Boudeulle *et al.* (23) and Greaves (24) was 0.833–0.834 nm. The change of color from black to dark brown and the temperature dependence of magnetization as described later also support the phase change of the films from Fe_3O_4 to γ-Fe_2O_3. The crystallite size derived from the full width at half maximum of the *hhh* reflection using the Hall method (25) was both 46 nm for the films before and after oxidation. This means that there was very little growth of crystallite size during the oxidation process. The Hall method also exhibited that the broadening of the *hhh* peaks with increasing 2θ angles implies nonuniform distortion, i.e., the disorder of the d spacings, of the (111) plane.

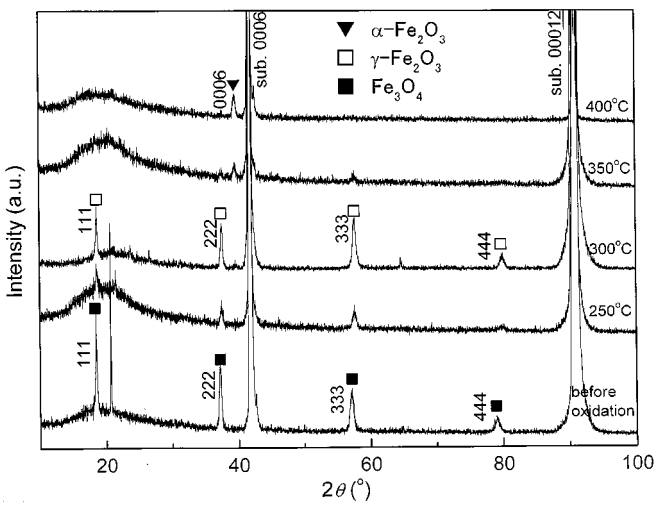

FIG. 3. XRD patterns of films before and after oxidation of the epitaxial Fe_3O_4 (111) films at 250–400°C in air flow.

D. *Epitaxial Relationship between the Fe_3O_4 and γ-Fe_2O_3 Films and the α-Al_2O_3 Substrate*

The conventional XRD θ–2θ scanning provides information on the d spacings only along the direction perpendicular to the substrate surface; thus we cannot estimate the in-plane alignment of the films from these θ–2θ scan data. Therefore, we carried out pole-figure measurement, in which the films are tilted (ψ) and rotated (ϕ) at a specified θ–2θ angle, in order to investigate the in-plane alignment of films. A pole figure using the α-Fe_2O_3 $10\bar{1}4$ reflection for the film on α-Al_2O_3 (0001) after heat treatment at 800°C in air is shown in Fig. 4a. The film is highly in-plane aligned because it exhibited distinct three spots. The appearance of these three spots corresponds to corundum structure, in which the c-axis is the axis of threefold rotation.

Similarly, pole-figure analysis was carried out using the Fe_3O_4 400 reflection for the film reduced at 330°C under a pH_2 of 0.023 atm. Instead of three spots, six sharp spots corresponding to the sixfold symmetry were observed at $\psi \sim 55°$ in the pole figure for the film (Fig. 4b). If the films were fully single crystalline, only three spots would be observed at 120° intervals of ϕ because of threefold symmetry relative to the [111] axis. Hence, the pole figure suggests the occurrence of two variants or twinned in-plane alignments between which the angle is 60° or 180°. In other words, there are two kinds of stacking order of close-packed oxide anion layers, i.e., "ABCABC" and "ACBACB" (5). Figure 4c shows ϕ-scans for the α-Al_2O_3 substrate using the $10\bar{1}4$ reflection ($2\theta = 35.148°$, $\psi = 38.2°$) and for the Fe_3O_4 film using the 400 reflection ($2\theta = 43.05°$, $\psi = 54.8°$). From the relative peak positions of the scans, the crystallographic relationship was obtained: Fe_3O_4 (111)$\|\alpha$-Al_2O_3 (0001) and Fe_3O_4 $[1\bar{1}0]\|\alpha$-Al_2O_3 $\langle\bar{1}100\rangle$, $\langle 1\bar{1}00\rangle$, as illustrated in Fig. 5. The pole figures for the γ-Fe_2O_3 films oxidized at 200–300°C in air exhibited six spots (not shown here) similar to that for

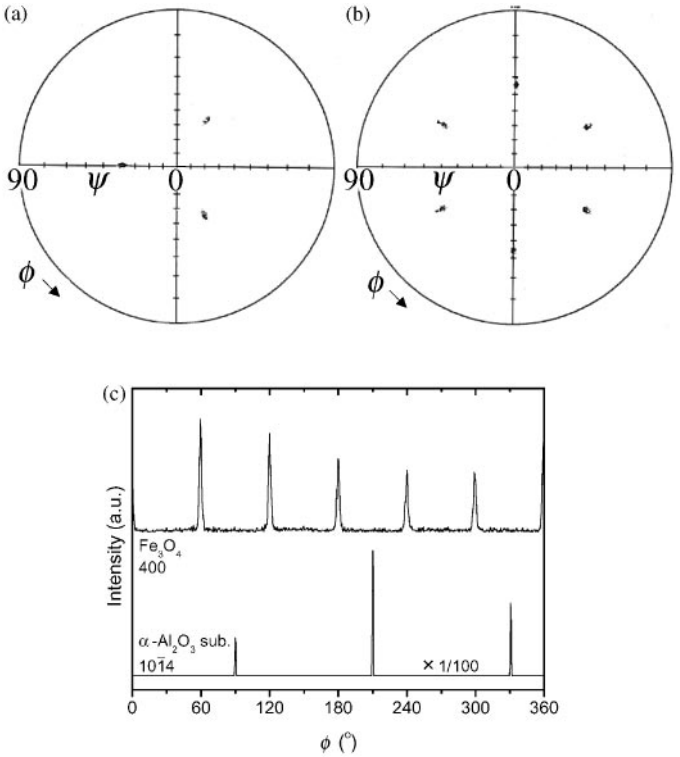

FIG. 4. XRD pole figures of (a) α-Fe_2O_3 film and (b) Fe_3O_4 film after reduction at 330°C, and (c) ϕ-scans of the Fe_3O_4 400 reflection and the α-Al_2O_3 10$\bar{1}$4 reflection for the reduced film.

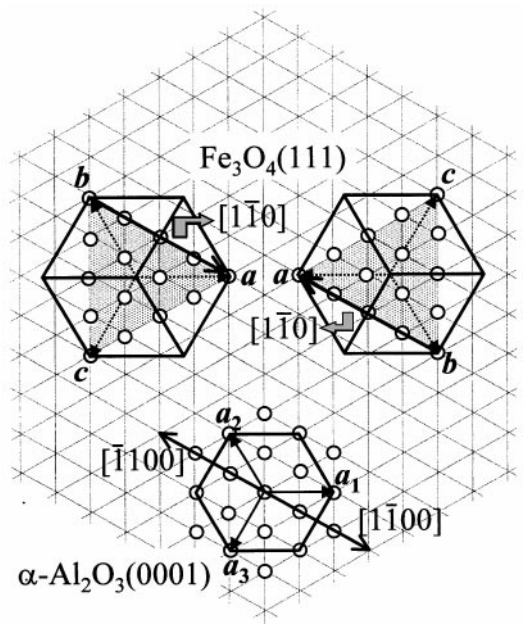

FIG. 5. The orientation relationship for two variants of epitaxial spinel (111) films on the corundum (0001) substrate.

the Fe_3O_4 films since γ-Fe_2O_3 has also the spinel-based structure.

Figure 6 shows (a) a pole figure and (b) ϕ-scans using the 10$\bar{1}$4 reflections for the α-Fe_2O_3 film regenerated from the γ-Fe_2O_3 through oxidation at 400°C in air. There appeared three comparatively strong spots with intervals of 120° and three weak spots at the midway between the former at $\psi = 38°$. Although weak owing to regeneration from γ-Fe_2O_3, the latter three peaks are clearly seen by careful measurement of the ϕ-scan (Fig. 6b). This means that most of the grains, which contribute to the stronger peaks, have epitaxially grown as the same arrangement with the α-Al_2O_3 substrate with a crystallographic relationship: α-Fe_2O_3 (0001) $\|$ α-Al_2O_3 (0001) and α-Fe_2O_3 $\langle 3000\rangle \| \alpha$-$Al_2O_3$ $\langle 3000\rangle$. In contrast, the rest of the grains, which correspond to the weaker spots, are 180° (or 60°) rotated variants of which the structural relationship is: α-Fe_2O_3 (0001) $\|$ α-Al_2O_3 (0001) and α-Fe_2O_3 $\langle \bar{3}000\rangle \|$ α-Al_2O_3 $\langle 3000\rangle$. Corundum structures have cations in two thirds of octahedral sites. Unoccupied octahedral sites stack "abcabc" along the [0001] axis. In the reoxidized α-Fe_2O_3 films on α-Al_2O_3, if the stacking sequence of unoccupied cation sites in the major grains is "abcabc", that in the minor grains is "acbacb", such as the twins observed in our previous V_2O_3 films (17). It is surprising that the intensities of the two variants are significantly different. Kachi *et al.* (26) found that when they annealed the bulk γ-Fe_2O_3 to form twinned α-Fe_2O_3 the twins disappeared if it was heated above 600°C. However, it is reasonable that twins have disappeared at higher temperatures since the presence of twins implies an excess interface energy and therefore is disadvantageous from the thermodynamic point of view. Similarly, in the present case of α-Fe_2O_3 regeneration, the topotactic reaction seems to be influenced by interface energy with substrate since the majority of grains have grown epitaxially and have the same cation arrangement as the substrate.

E. Magnetic Properties of Fe_3O_4 and γ-Fe_2O_3 Films

In this section, we discuss the magnetic properties of the Fe_3O_4 film after reduction of the α-Fe_2O_3 film at 330°C in $pH_2 = 0.023$ atm and of the γ-Fe_2O_3 film after oxidation of the Fe_3O_4 film at 300°C in air. The magnetic properties of Fe_3O_4 films at low temperatures have been investigated by a number of researchers (27). Fe_3O_4 undergoes a phase transition called the Verwey transition at ~ 120 K from cubic to monoclinic symmetry accompanied by the drastic change of electric conductivity as well as magnetization (28, 29). Figure 7 shows magnetization curves for the Fe_3O_4 and γ-Fe_2O_3 films measured by SQUID. A distinct change appeared at ~ 120 K in a magnetic field of 1000 Oe with rising temperature after cooling in zero-magnetic field for

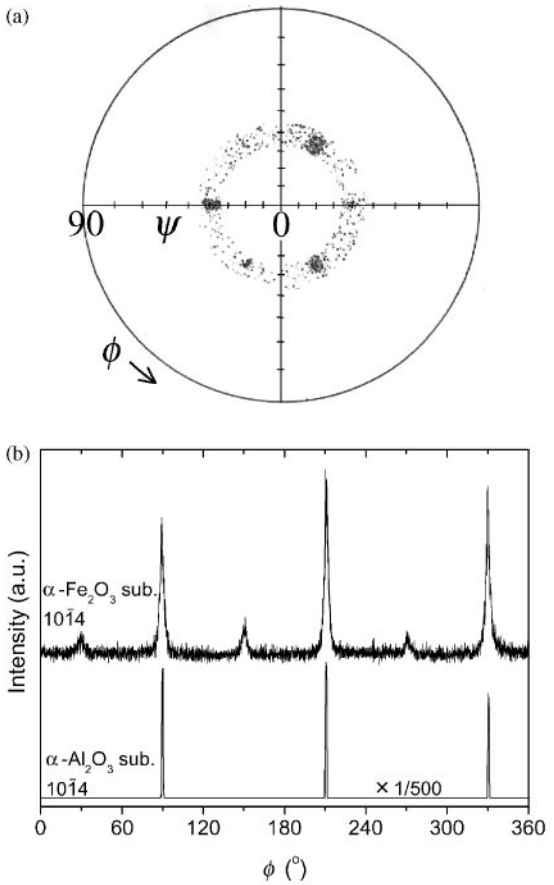

FIG. 6. XRD pole figure of (a) the α-Fe_2O_3 film after reoxidation at 400°C in air and (b) ϕ-scans of the 10$\bar{1}$4 reflection of α-Fe_2O_3 film and α-Al_2O_3 substrate.

the Fe_3O_4 film but not for the γ-Fe_2O_3 film. This is another evidence of Fe_3O_4 in the former film.

Moreover, Fig. 8 shows magnetization versus magnetic field (M–H) hysteresis loops for the Fe_3O_4 and γ-Fe_2O_3 films at 300 K. The magnetic field was applied to the direction parallel to the film surfaces. There was no perpendicular magnetization in the films. Saturation magnetizations are 24 and 15 emu/g for the Fe_3O_4 and γ-Fe_2O_3 films, respectively, which are lower than the bulk values (98 and 84 emu/g, respectively). The accuracy in evaluation of magnetization per gram of film depends on that of the weight of the film rather than the error accompanying the subtraction of the magnetization due to the substrate from the measured value. Since the weight of the films was in the order of 10^{-2} mg, which corresponds to $\sim 0.5\%$ of that of the substrates, the accuracy of magnetization per gram of film is one order of magnitude. Another reason for the difference is the cation disorder, or disorder of d-spacings as implied by broadening of the FWHM of XRD peaks using the Hall method in section C, caused by a strongly reductive condition. If this is the case, saturation magnetization of the

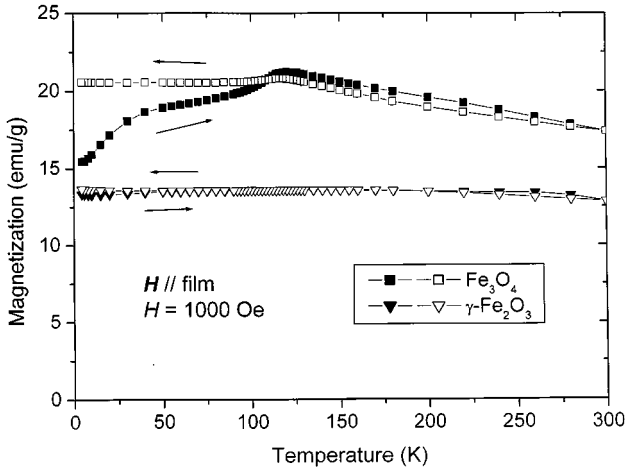

FIG. 7. Temperature dependence of magnetization for Fe_3O_4 and γ-Fe_2O_3 films.

film will approach the bulk value when the film is postannealed in the Fe_3O_4 stable region. On the other hand, magnetic coercivities (H_c) were 500 and 250 Oe for the Fe_3O_4 and γ-Fe_2O_3 films, respectively, which were almost identical with those of some (111)-preferred films (12, 30, 31). An average crystallite size estimated by XRD was 46 nm, which is considered to be below the single-domain size. However, grain sizes by AFM observation were 100–300 nm as will be shown later. These were consistent with those obtained by Schmitdbauer *et al.*, i.e., ~ 250 nm (32). The origin of high H_c value of the films may be the shape, crystalline, or stress-induced magnetic anisotropy; however, further research is needed to discuss the details.

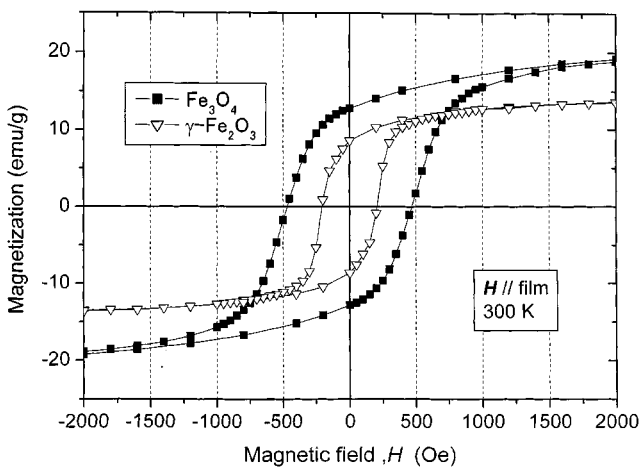

FIG. 8. Magnetic hysteresis curves of Fe_3O_4 and γ-Fe_2O_3 films at 300 K.

F. Observations of Surface Morphology by Atomic Force Microscopy

Figure 9 shows AFM images in the height (left) and deflection (right) modes of (a) α-Fe_2O_3, (b) Fe_3O_4, and (c) γ-Fe_2O_3 films. In these modes the probe (cantilever) is scanned as follows. The force applied to the cantilever is changed as the roughness of surface varies. The height image is constructed by the sample height (position) accommodated as the force (deflection) is constant and expresses literally the height itself. By contrast, the deflection image is constructed by the deflection intensity of cantilever at the roughness. Thus, an edge of a particle can be more clearly seen in the deflection image. In Fig. 9a, a number of steps were observed in the α-Fe_2O_3 film, of which the flat surfaces correspond to the α-Fe_2O_3 (0001) basal plane. In contrast, the surface of the Fe_3O_4 and γ-Fe_2O_3 films became blunt, as shown in Figs. 9b and 9c, respectively. Such disappearance of distinct steps is attributable not only to the volume change accompanying the phase changes from α-Fe_2O_3 to Fe_3O_4 and to γ-Fe_2O_3 but to isotropic nature of the cubic lattice in the latter spinel-type oxides. Therefore, in the latter films, perpendicular magnetization due to the shape anisotropy is not to be expected. The observed grain sizes were in the order of 100–300 nm. This suggests that no increase or decrease in size has occurred during the redox reactions. However, the grains in the γ-Fe_2O_3 film appeared to consist of aggregation of primary particles with a diameter of $\sim$ 10 nm (Fig. 9c). A number of fine pores and microcracks along the grain boundaries were observed in its deflection image. The occurrence of such pores and cracks is assumed to originate from the volume change from Fe_3O_4 to γ-Fe_2O_3 and oxygen transport is enhanced through these pores.

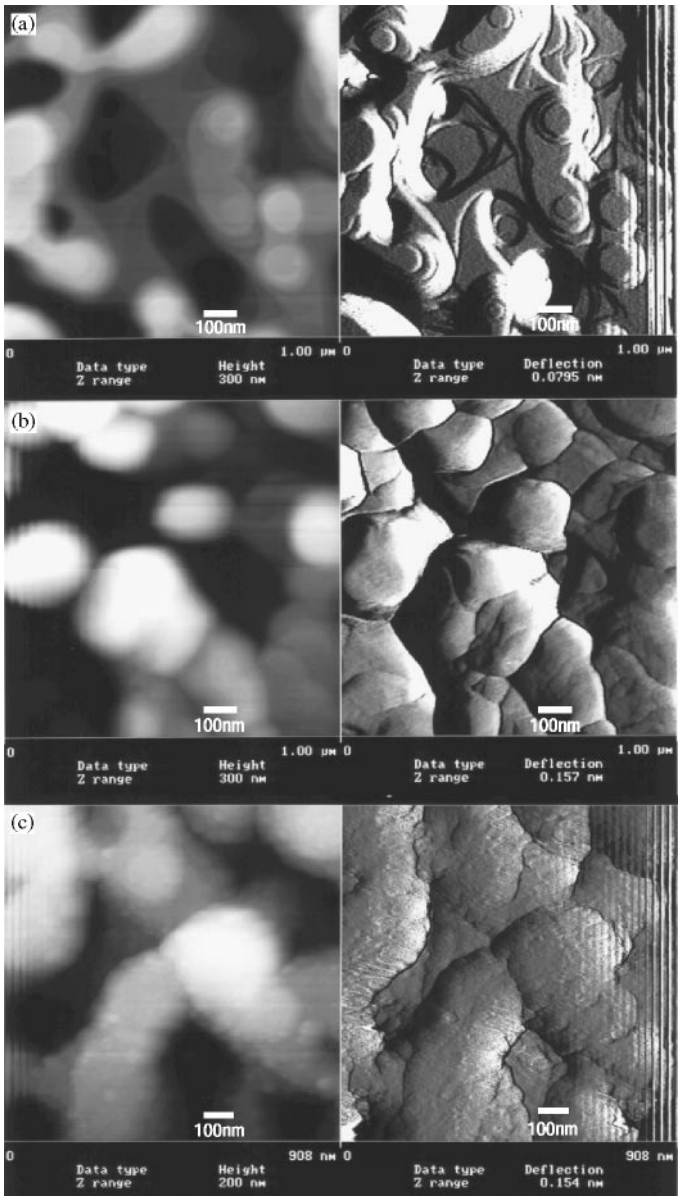

FIG. 9. AFM observations of (a) α-Fe_2O_3, (b) Fe_3O_4, and (c) γ-Fe_2O_3 films. Left and right images correspond to height and deflection modes, respectively.

G. Structural Transformation between Corundum-Type and Spinel-Type Iron Oxides: Advantages of PET Process

Spinel and corundum structures have different oxide anion sublattices as described earlier. Close packed layers of oxide anions stack in the sequence ABCABC in the spinel-type and in the sequence ABABAB in the corundum-type compounds. That is, migration of oxide anions that have a comparatively large ion radius is required. Therefore, the conversion from α-Fe_2O_3 to Fe_3O_4 requires a larger energy than that from Fe_3O_4 to γ-Fe_2O_3 in which migration of small cations only is needed. Kachi *et al.* (26) and Mathieu *et al.* (33) discussed cooperative transfer of oxide anions and iron cations during the γ- to α-Fe_2O_3 transition. The displacement of oxide anion accompanying the transformation from α-Fe_2O_3 to Fe_3O_4 is considered to be similar to the reverse reaction from γ- to α-Fe_2O_3 transition as shown in Fig. 10. That is, each pair of oxide layers with one iron layer between them cooperatively glide with a translation step of $a_{hem}/3$ along the direction $\langle 3000 \rangle$ or $\langle \bar{3}000 \rangle$, the basal plane being the glide plane. The number of iron cations between the pair of oxide layers in Fe_3O_4, $\frac{3}{4}$, is different from that in α-Fe_2O_3, $\frac{2}{3}$. Therefore, cations must transverse across oxide layers. Further work such as atomic image observations using transmission electron microscopy will be needed to discuss the refined reaction mechanism, however, we presume that some cooperative transfer of ions occurs to help the topotactic transformation between the corundum-type and spinel-type iron oxides.

Finally, reaction schemes that are included in this article are shown in Fig. 11. Bold arrows represent postepitaxial

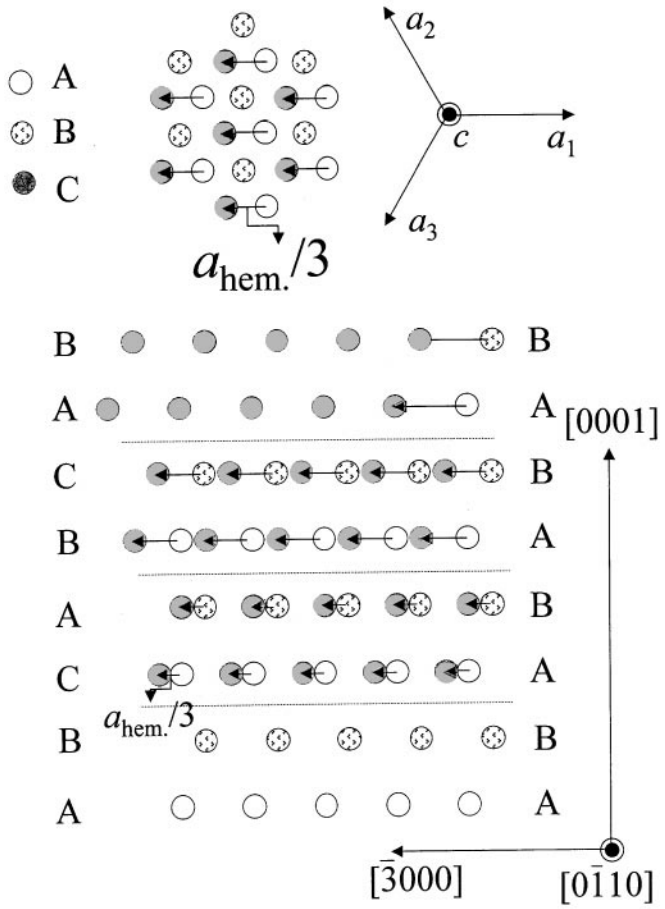

FIG. 10. Schematic displacement of close-packed oxide layers in the topotactic transition from α-Fe_2O_3 to Fe_3O_4. (adapted from Kachi *et al.* (26)).

topotaxy routes. On the other hand, epitaxial growth of Fe_3O_4(111) films on α-Al_2O_3(0001) via an amorphous phase is unlikely. This is suggested by the following two results. First, no amorphous phase was observed in the XRD θ–2θ scans for the film reduced with H_2 as shown in Fig. 2. Second, epitaxial Fe_3O_4 was produced by reduction of an epitaxial α-Fe_2O_3 film (Fig. 2), whereas it could not be directly obtained from the as-prefired amorphous precursor films (Fig. 1b). Of course, formation of an amorphous phase and disappearance of long-range order on a microscopic scale might have occurred, however, the crystallographic relationship, i.e., the spinel (111) plane ∥ the corundum (0001) plane, has been maintained during the redox reactions between iron oxides in the present study. Therefore, our postepitaxial topotaxy (PET) process, in which one epitaxial film is topotactically converted to another epitaxial film, is a very versatile method to prepare epitaxial films, especially on a substrate having a different type of crystal structure or a large lattice mismatch.

CONCLUSIONS

We have succeeded in preparation of (111)-oriented epitaxial magnetite (Fe_3O_4) films on C-planes of sapphire [α-Al_2O_3(0001)] by a postepitaxial topotaxy (PET) process using only chemical methods. In this process, first, (0001)-oriented epitaxial hematite (α-Fe_2O_3) films were prepared on the substrate by a coating-pyrolysis process. The crystallographic relationship of the film and substrate was α-Fe_2O_3 (0001) ∥ α-Al_2O_3 (0001) and α-Fe_2O_3 ⟨3000⟩ ∥ α-Al_2O_3 ⟨3000⟩. Second, the α-Fe_2O_3 films were reduced in

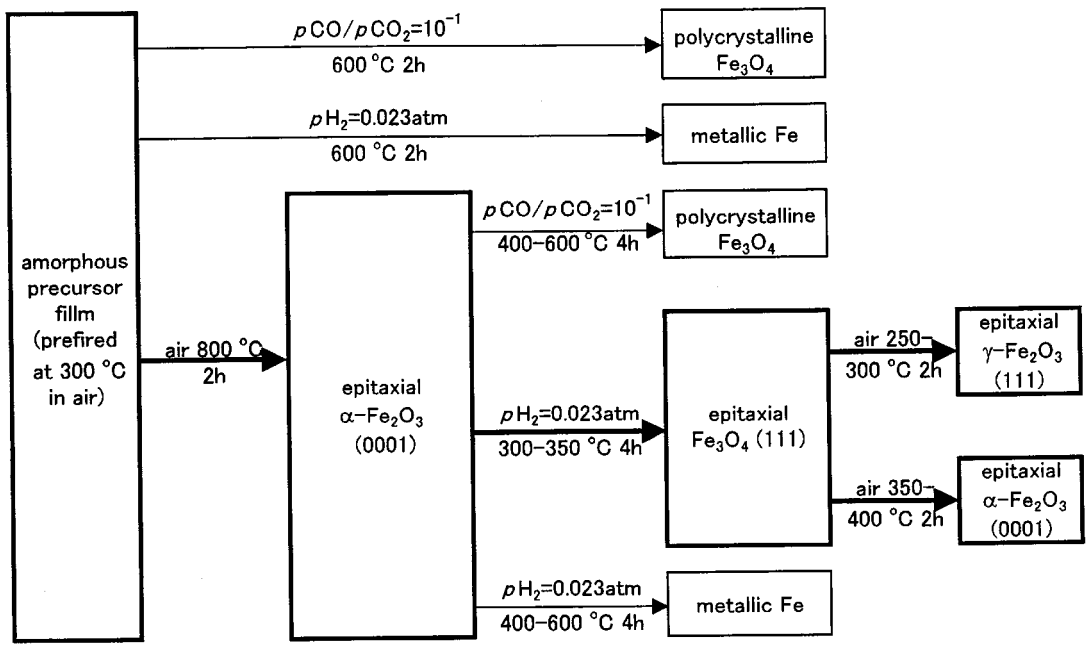

FIG. 11. Reaction schemes that are included in this article. Bold arrows represent postepitaxial topotaxy routes.

an $Ar–H_2$ atmosphere ($pH_2 = 0.023$ atm) to Fe_3O_4 films. Pole-figure analysis exhibited that the Fe_3O_4 films were (111)-oriented epitaxial films. Two variants of Fe_3O_4 grains occurred and their crystallographic relationships were Fe_3O_4 (111) $\|$ α-Al_2O_3 (0001) and Fe_3O_4 [$1\bar{1}0$] $\|$ α-Al_2O_3 $\langle 1\bar{1}00\rangle$, $\langle \bar{1}100\rangle$. That is, α-Fe_2O_3 has been converted to Fe_3O_4 topotactically. Finally, epitaxial Fe_3O_4 films were oxidized in air to epitaxial γ-Fe_2O_3 films topotactically.

Fe_3O_4 has a spinel-type structure with fcc sublattice of oxide anions, whereas α-Al_2O_3 has a corundum-type structure with hcp sublattice of oxide anions, the lattice mismatch being 8.0%. This present results exhibited that the topotactic reaction of epitaxial films (PET process) is particularly useful for the following cases: (i) the structure type of the film is different from that of the substrate, and (ii) the lattice mismatch with the substrate is large. Although the PET process will also be applicable to thin film preparation by gas-phase deposition methods, we think that the process will find a wider applications in the thick film fabrication by chemical solution-based routes since, using the latter processes, epitaxy has been thought quite difficult to obtain with such a set of film and substrate.

REFERENCES

1. For example, Epitaxial Oxide Thin Films III. *Mater. Res. Soc. Symp. Proc.* **474** (1997).
2. T. Manabe, W. Kondo, S. Mizuta, and T. Kumagai, *J. Mater. Res.* **9,** 858 (1994).
3. T. Nagahama, T. Manabe, I. Yamaguchi, T. Kumagai, S. Mizuta, and T. Tsuchiya, *J. Mater. Res.* **15,** 783 (2000).
4. T. Manabe, I. Yamaguchi, W. Kondo, S. Mizuta, and T. Kumagai, *J. Mater. Res.* **12,** 541 (1997).
5. Y. Gao, Y. J. Kim, S. A. Chambers, and G. Bai, *J. Vac. Sci. Tech. A* **15,** 332 (1997).
6. T. Fujii, M. Takano, R. Katano, Y. Isozumi, and Y. Bando, *J. Magn. Magn. Mater.* **130,** 267 (1994).
7. I. Yamaguchi, T. Manabe, T. Kumagai, W. Kondo, and S. Mizuta, *J. Mater. Res.* **13,** 935 (1998).
8. I. Yamaguchi, T. Manabe, T. Kumagai, W. Kondo, and S. Mizuta, *Thin Solid Films* **365,** 36 (2000).
9. T. A. Derouin, C. D. E. Lakeman, X. H. Wu, J. S. Speck, and F. F. Lange, *J. Mater. Res.* **12,** 1391 (1997).
10. T. Fujii, M. Takano, R. Katano, Y. Bando, and Y. Isozumi, *J. Appl. Phys.* **66,** 3168 (1989).
11. T. Fujii, M. Takano, R. Katano, Y. Bando, and Y. Isozumi, *J. Appl. Phys.* **68,** 1735 (1990).
12. H. J. Masterson, J. G. Lunney, and J. M. D. Coey, *J. Magn. Magn. Mater.* **115,** 155 (1992).
13. D. Zscherpel, W. Ranke, W. Weiss, and R. Schlögl, *J. Chem. Phys.* **108,** 9506 (1998).
14. Y. J. Kim, C. Westphal, R. X. Ynzunza, Z. Wang, H. C. Galloway, M. Salmeron, M. A. Van Hove, and C. S. Fadley, *Surf. Sci.* **416,** 68 (1998).
15. Y. Q. Cai, M. Ritter, W. Weiss, and A. M. Bradshaw, *Phys. Rev. B* **58,** 5043 (1998).
16. I. Yamaguchi, T. Terayama, T. Manabe, T. Kumagai, and S. Mizuta, *J. Sol-Gel Sci. Tech.* **19,** 753 (2000).
17. I. Yamaguchi, T. Manabe, T. Kumagai, W. Kondo, and S. Mizuta, *Thin Solid Films* **366,** 294 (2000).
18. K. Tamari, T. Doi, and N. Horiishi, *Appl. Phys. Lett.* **63,** 3227 (1993).
19. M. Ozaki, S. Kratohvil, and E. Mtijevic, *J. Colloid Interface Sci.* **102,** 146 (1984).
20. C. Li and Z. Hong, *J. Solid State Chem.* **134,** 248 (1997).
21. M. Ozaki and E. Matijevic, *J. Colloid Interface Sci.* **107,** 199 (1985).
22. D. R. Gaskell, *in* "Introduction to Metallurgical Thermodynamics," p. 442. McGraw-Hill Kogakusha, Tokyo, 1973.
23. M. Boudeulle, H. Batis-Landoulsi, CH. Leclercq, and P. Vergnon, *J. Solid State Chem.* **48,** 21 (1983).
24. C. Greaves, *J. Solid State Chem.* **49,** 325 (1983).
25. W. H. Hall, *Proc. Phys. Soc. A* **62,** 741 (1949).
26. S. Kachi, K. Momiyama, and S. Shimizu, *J. Phys. Soc. Jpn.* **18,** 106 (1963).
27. D. T. Margulies, F. T. Parker, F. E. Spada, R. S. Goldman, J. Li, R. Sinclair, and A. E. Berkowitz, *Phys. Rev. B* **53,** 9175 (1996).
28. E. J. W. Verwey, *Nature* **144,** 327 (1939).
29. M. Matsui, S. Todo, and S. Chikazumi, *J. Phys. Soc. Jpn.* **43,** 47 (1977).
30. J. K. Lin, J. M. Sivertsen, and J. H. Judy, *J. Appl. Phys.* **57,** 4000 (1985).
31. Z.-J. Zhou and J.-J. Yan, *J. Magn. Magn. Mater.* **115,** 87 (1992).
32. E. Schmidbauer and R. Keller, *J. Magn. Magn. Mater.* **152,** 99 (1996).
33. F. Mathieu and A. Rousset, *Phil. Mag. A* **67,** 533 (1993).